Symmetry controlled excited state dynamics

Journal:	*Physical Chemistry Chemical Physics*
Manuscript ID	CP-ART-09-2018-005950.R2
Article Type:	Paper
Date Submitted by the Author:	27-Oct-2018

Complete List of Authors:	Waters, Max; University of Copenhagen, Department of Chemistry Skov, Anders; University of Copenhagen, Department of Chemistry Larsen, Martin; Kobenhavns Universitet Det Natur- og Biovidenskabelige Fakultet, Department of Chemistry Weber, Peter; Brown University, Dept. of Chemistry Clausen, Christian; University of Copenhagen, Department of Chemistry Sølling, Theis; Kobenhavns Universitet Det Natur- og Biovidenskabelige Fakultet, Department of Chemistry

Journal Name

ARTICLE TYPE

Cite this: DOI: 10.1039/xxxxxxxxxx

Symmetry controlled excited state dynamics†

Max D.J. Waters,[a] Anders B. Skov,[a] Martin A.B. Larsen,[a] Christian M. Clausen,[a] Peter M. Weber,[b] and Theis I. Sølling*[a]

Received Date
Accepted Date

DOI: 10.1039/xxxxxxxxxx

www.rsc.org/journalname

Symmetry effects in internal conversion are studied by means of two isomeric cyclic tertiary aliphatic amines in a velocity map imaging (VMI) experiment on the femtosecond timescale. It is demonstrated that there is a delicate structural dependence on when the coherence is preserved after the transition between the 3p and 3s Rydberg states. N-methyl morpholine (NMM) shows unambiguous preserved coherence, consistent with previous work, which is decidedly switched off by the repositioning of oxygen within the ring. From the differences in these dynamics, and an examination of the potential energy surface following the normal modes of vibration, it becomes clear that there is a striking dependence on atom substitution, which manifests itself in the permitted modes of vibration that take the system out of the Franck-Condon region through to the 3s minimum. It is shown that the non Fermi-like behaviour of NMM is due to a conical intersection (CI) between the $3p_x$ and 3s states lying directly along the symmetry allowed path of steepest descent out of the Franck-Condon region. NMI, where the symmetry has been changed, is shown to undergo internal conversion in a more Fermi-like manner as the energy spreads through the available modes ergodically.

1 Introduction

Understanding how light interacts with matter, and the resulting flow of energy through a molecular system, is key to approaching the design of molecules with the goal of tuning their properties for specific photochemical, or electronic, applications. With the advent of ultrafast spectroscopy it is possible to examine the degree of coupling between states as a function of molecular structure. The aim of this work is to address how subtle symmetry changes can impact the flow of internal energy.

Fermi's golden rule is often invoked to describe internal conversion in a system[1], as it can give an approximate value for the rate of internal conversion in systems that behave in a statistical manner. In that case, the transition probability $\Gamma_{i\to f}$ is given by

$$\Gamma_{i\to f} = \frac{2\pi}{\hbar} |\langle \Psi_i | H' | \Psi_f \rangle|^2 \rho \qquad (1)$$

Where Ψ_i and Ψ_f are the wavefunctions of the initial and final states, respectively. The degree of overlap between the is expressed by the matrix element $\langle \Psi_i | H' | \Psi_f \rangle$ of the perturbing Hamiltonian H', and the density of final states is given by ρ. In standard Fermi-like systems, the system explores the available degrees of freedom in a statistical manner, and the rate of internal conversion can largely be discussed purely in terms of the density of states available in the receiving state. Using this rule, one concludes that systems with lower symmetry undergo internal conversion on faster timescales than analogous systems with higher orders of symmetry, simply due to the greater density of states that the system would be permitted to transition into; however, in the two molecules presented in this work it is clearly shown that by breaking the symmetry from one regioisomer to another, one changes the behaviour of the internal conversion from a more statistical, non-coherent process to a non-statistical, coherent process.

It has been understood for some time that ultrafast internal conversion can be driven by a non-ergodic evolution of the wavepacket on an excited state surface[2], meaning that the motion out of the Franck-Condon region and any subsequent excited state dynamics are non-statistical. Non-linear molecules have 3N-6 modes of vibration so that for a large non-linear molecule, it is exceptionally rare that a single normal mode is entirely responsible for the motion between two electronic states. In fact, a conical intersection (CI) requires at least two degeneracy-lifting degrees of freedom[3] and in molecules with such large degrees of freedom, isolating and understanding the dynamics of how a chemical system passes through a CI is a non-trivial task[4]. Determining which molecular vibrations are responsible for these transitions

[a] Department of Chemistry, University of Copenhagen, Universitetsparken 5, 2100 Copenhagen Ø, Denmark. Fax: +45 35 32 03 22; Tel: +45 93 56 54 72; E-mail: theis@chem.ku.dk
[b] Department of Chemistry, Brown University, Providence, RI 02912, U.S.A.

† Electronic Supplementary Information (ESI) available: [details of any supplementary information available should be included here]. See DOI: 10.1039/b000000x/

has allowed us in the past to gain deeper insight into predicting, interpreting, and understanding chemistry, as well as more nuanced methods of modelling and analysing how a wavepacket can move, or be directed, around a potential energy surface (PES) [5,6].

Indeed, observing preserved structural coherence in a system is not a new phenomenon - having first been reported by Zewail [7] in sodium iodide. However, it is still rare that similar observations are made in much larger systems [8,9], and only very recently has the same phenomena been reported after the system has undergone internal conversion [10,11]. Internal conversion between excited states is an area of physical chemistry and chemical physics that consistently generates interest due to the fact that it is a process that can foster efficient energy conversion from excited state potential energy into nuclear kinetic energy, without losing any energy through radiation [12]. This makes molecules that can undergo efficient internal conversion particularly attractive for any technology pertaining to storage of solar energy [13] or molecular photoswitches [14].

In addition to the work conducted by Zewail, many previous studies have shown that internal conversion is often driven by a small set of normal modes in large polyatomic systems [15–20], though this work has been, for the large part, theoretical without presenting much experimental data. This phenomenon of internal conversion being driven by a small number of modes is the basis of the photophysics presented in this work, as the coupling the the 3p manifold and 3s Rydberg state in both NMM and NMI occurs along the amine wagging motion and carbon nitrogen stretching motion. However, what makes it most interesting in these amine systems is that the ion and Rydberg states have been long considered to be parallel to each other, which should make the observation of any vibrational coherence impossible. The previous work by Zhang et al. [11] demonstrated that this previous interpretation is not valid.

Central to internal conversion is the idea of the CI, which is to say that there may be a region of the PES where the system has a nuclear geometry which leads to the degeneracy of two or more electronic surfaces. Through work conducted by Yarkony et al. [21], and the combined efforts of Robb, Olivucci, and Bernardi [22–24] it has been shown that CIs are ubiquitous in ultrafast dynamics. With this in mind, it is therefore interesting that oscillations in NMM are due to one specific normal mode, whilst a scan of the relevant excited state PESs along this mode shows that they are near parallel, with no topology that would indicate any non-adiabatic behaviour. One established way in which it is possible for Rydberg states to undergo ultrafast internal conversion is through Rydberg-valence mixing [25,26] in which a distortion of the molecular structure causes it to acquire significant valence character, meaning that enough of the electron density is located in an antibonding orbital to cause the topology of the PES to differ noticeably from that of the ion state.

In the ongoing investigation of the photodynamics of tertiary aliphatic amines, and the nature of the transition between the 3p and 3s Rydberg states, Zhang et al. [11] showed that in NMM there is a preserved coherence along the amine umbrella mode. Observation of coherent oscillations in the time-resolved photoelectron imaging (TRPEI) spectrum is not only interesting from a dynamics point of view, it also represents a significant break from the typical interpretation of excited amines [27]. Initially, it was thought that it would not be possible to resolve oscillations that are due to structural coherences in these systems due to the fact that Rydberg and ion states are commonly thought of as being parallel to each other (or near-parallel to such an extent that the gradient differences would not be able to be resolved) due to progressively higher lying Rydberg states having increasingly diffuse and extended wavefunctions, until they converge with the ion state [28]. This would mean that there would be no change in energy difference along the coordinate of oscillation, implying that oscillations would not be observed. The scope of studies into tertiary aliphatic amines, both cyclic and non-cyclic, has been broad and yet (to the best knowledge of the authors) structural coherences in this class of compounds had not been observed until this point [27,29–31]. This is not the case in other systems where structural coherences have been observed, such as *o*-fluorophenol [9], due to the ion state, D_0, being more similar in topology to the ground state, S_0, than the double-well excited state, 3s. From the recent finding in NMM it is clear that this is not the case in some amines as well.

In this present study, a contrast and comparison is drawn between N-methyl isomorpholine (NMI) and N-methyl morpholine (NMM), both shown in figure 1, with the goal of understanding the impact of symmetry upon the dynamics of NMM and how it can be a controlling factor for the preservation of vibrational coherence during internal conversion. The results that have been previously observed [11] were replicated and it was demonstrated that this surprising behaviour is not present in NMI. Therefore, the structure of NMM must inherently be less conducive to coupling between normal modes than that of NMI. Presented here are some arguments based on experimental evidence and calculations that demonstrate that this is likely the explanation for the observation of coherent oscillations in the case of NMM whilst these are not observed in the NMI spectrum.

2 Methodology

2.1 Experimental Methods

The Copenhagen VMI setup has been described in detail elsewhere [29]. NMM was purchased from Sigma-Aldrich (99% purity). 3-methyl-1-oxa-3-azinane (NMI) was synthesized according to the procedure by Katritzky and coworkers with modifications for the workup [33]. The NMR spectral data associated with the synthesis is provided as supporting information in figures $1^{\dagger}$-$3^{\dagger}$. The synthesis afforded NMI with a 28% impurity of methanol, which is not expected to affect the pump-probe data due to methanol not having any absorption of either pump or probe through a single-photon process. Any multi-photon absorption is not expected to play a role, as two-photon absorption at 200 nm will lead directly to ionization ($E_{2\times 200\,nm} = 12.4\,eV$ [34], $IE_{MeOH} = 10.84\,eV$ [35]) giving a non-time dependent signal which is subtracted during data analysis. Furthermore a three-photon absorption at 400 nm will only give signal at negative time delays, and will have a very low intensity in comparison to the single-photon absorption response of NMI.

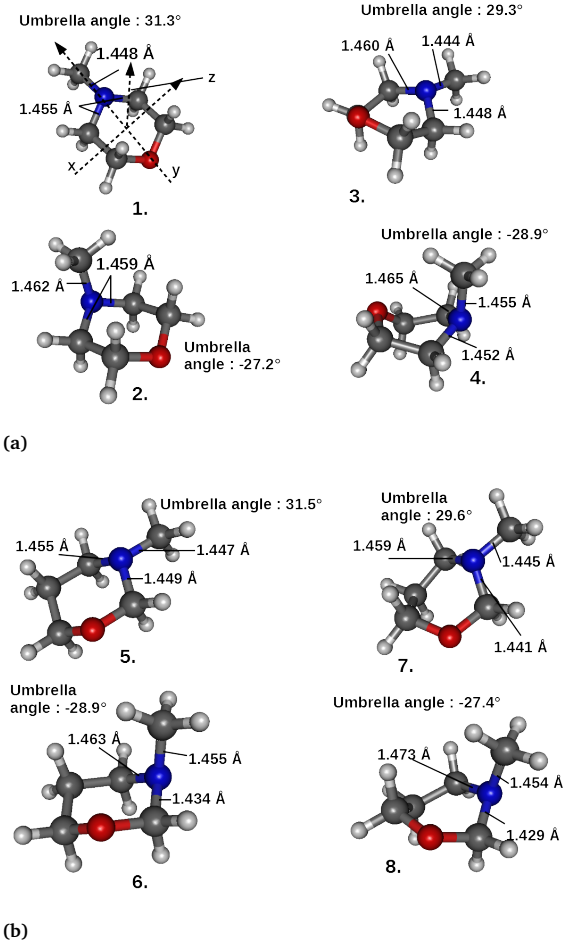

Fig. 1 Ground state structures[32] of the minima of a) NMM and b) NMI calculated with CAM-B3LYP/6-311++G(d,p), both are in a equatorial chair conformation. In each molecule, structure 1. corresponds to the equatorial chair, as it is in a chair conformation whilst the methyl is equatorial. The rest of the structures are labelled following the same scheme, 2. is labelled axial chair, 3. equatorial boat, 4. axial boat. The umbrella angle tells us to what degree the nitrogen is planarised, a value of 0° would mean that the nitrogen centre is completely planar.

A vapour phase UV-Vis spectrum was taken of NMI using a Varian Cary 50 UV-Vis Spectrophotometer, to determine the absorption band. NMM and NMI were examined in the gas phase using ultrafast VMI with a pump wavelength of 200 nm and a probe wavelength of 400 nm. The pump beam was generated using fourth harmonic generation from an 800 nm fundamental, whilst the probe beam was generated via second harmonic generation.

2.2 Computational Methods

In order to obtain an overview of the systems of interest, TD-DFT was employed (CAM-B3LYP/6-311++G(d,p)) using the Gaussian 16 program package[36]. CAM-B3LYP was chosen as it is known to give a good description of Rydberg states[37], and the initial calculations of excitation energies agreed well with the measured UV/Vis spectrum, as demonstrated in figure 2 and table 1. Stationary points on the ground, 3s Rydberg, and $3p_{x,y,z}$ Rydberg states were located and characterised by examining their frequencies. The PES was calculated following the normal modes. In addition to this, a relaxed scan following the methyl stretching coordinate was also calculated which resulted in the appearance of a crossing. Due to the notoriety of TD-DFT as an inadequate method for the characterisation of conical intersections (albeit for those between the ground state and excited states[38]), the intersection geometry was optimised and characterised at the CASSCF(12,12)/aug-cc-pVTZ level of theory. The active space was chosen to include the MOs and electrons involved in C-N bonding, the nitrogen lone pair, and both lone pairs on the oxygen atom because the HOMO is the nitrogen lone pair, and the C-N bonds were important to include due to the hypothesis of Rydberg-valence interaction playing a role. The oxygen lone pairs were included because the position of the oxygen was varied between the two molecules, making it important to be reflected in the active space. The CASSCF calculations were completed using the Molcas 8.0 program package[39], and the NMM conical intersection was characterised according to the method laid out by Galván et al[40]. Once there was verification that multireference methods were giving qualitative agreement with the results of the TD-DFT calculations, relaxed scans of the C-N bonds on both systems were calculated at the CAM-B3LYP/6-311++G(d,p) level of theory.

3 Results and Discussion

3.1 Experimental Results

A gas-phase steady state UV/Vis spectrum for NMI is shown in figure 2, demonstrating that there is a strong absorption at 200 nm which is assigned to the transition from the ground state to a 3p state. This is confirmed by *ab initio* calculations, which give a vertical transition of 199 nm. A small shoulder can also be seen at 211 nm, corresponding to a weak transition to the 3s state. The VMI spectra for NMM and NMI are shown in figure 3, and the ground state optimised structures are shown in figure 1. In essence, the main difference between the ground state minimum and the excited state minima is the configuration around the nitrogen. With the Rydberg species resembling the ionised species (at N) the preference is a planar configuration, and thus the transition from the Franck-Condon region to the minimum region is a planarisation of nitrogen. The TRPEI spectra show that, in each molecule, a 3p state is initially populated which then decays to the 3s state. Oscillations are clearly seen in the NMM spectrum, as was previously reported, which are not present in NMI. There is also a significant difference in the 3p lifetime of each molecule, with NMM decaying significantly faster than NMI.

Table 1 presents an overview and characterisation of the various minima present in each of the two systems. Due to the significant energy barriers from one minimum to another on the ground state in NMM, it can be assumed that the equatorial chair conformation dominates. In NMI there are two conformers that could be relevant, the equatorial chair or the axial chair. These conformers are both very close in energy, with very similar excitation energies. It should also be noted that these structures are minima that fall along the surface following the amine wagging motion on the ground state, so the transition state between them is likely

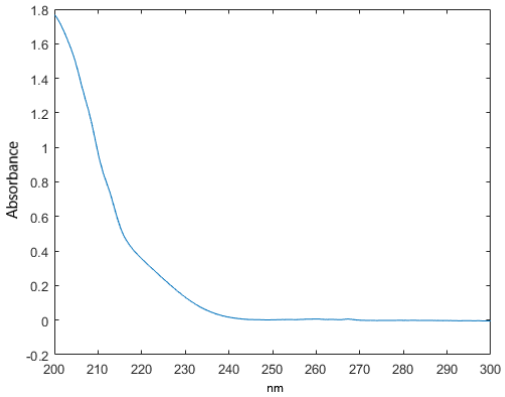

Fig. 2 Gas phase steady state UV-Vis absorption spectrum of NMI.

very small and easily overcome at room temperature. This could be the reason for the broad appearance of the peak associated with the n→3s transition in Figure 3a.

With an excitation pulse of 200 nm (FWHM 3.5 nm), the molecule can be excited to any of the 3p states in both NMI and NMM when in the conformers discussed above. In NMM symmetry restricts which vibronic transitions can occur, as the electronic ground state is $1^1A'$, implying that any transition to a $^1A''$ state requires the transition dipole moment to be perpendicular to the plane of the molecule.

The fit of the decay from 3p to 3s was obtained by integrating, and normalising the calibrated intensities between 0.5 and 1.0 eV for NMI, and 0.5 and 0.9 eV for NMM. A larger integration range was used for NMI as the 3p peak is more diffuse and is observed over a greater range than in NMM. A fit for the trace that was given from this was then obtained by the following function:

$$f(t) = A \cdot e^{-\frac{t}{\tau_{IC}}} \otimes g(t) \quad (2)$$

Where τ_{IC} is the internal conversion time constant, A is the signal amplitude, and $g(t)$ is the instrument response function. The oscillations in NMM were fitted separately by using the range 0.15 to 0.3 eV in the calibrated intensities to integrate over. The time trace was then fitted using the same function as before, but with the inclusion of an oscillating term:

$$f(t) = e^{\frac{-t}{\tau_{IC}}} \cdot \left[A_1 + A_2 \cdot \cos\left(\frac{2\pi t}{T} + \phi\right)\right] \quad (3)$$

On an initial examination, it seems reasonable to assume that the driving force for any excited state dynamics present in these molecules would be the amine umbrella mode simply based on the optimised structures for the ground and excited states. However when examining the PES along this mode it becomes clear that there is nothing to suggest ultrafast dynamics in either of these molecules. This stands in contrast to the experimental finding that both of the molecules studied relax from a 3p Rydberg state to the 3s Rydberg state within a few hundred femtoseconds.

Table 2 shows the lifetimes of the 3p state, as well as the oscillation periods for NMI and NMM. The 3p Rydberg state of NMI is longer lived than that of NMM, indicating that internal conversion

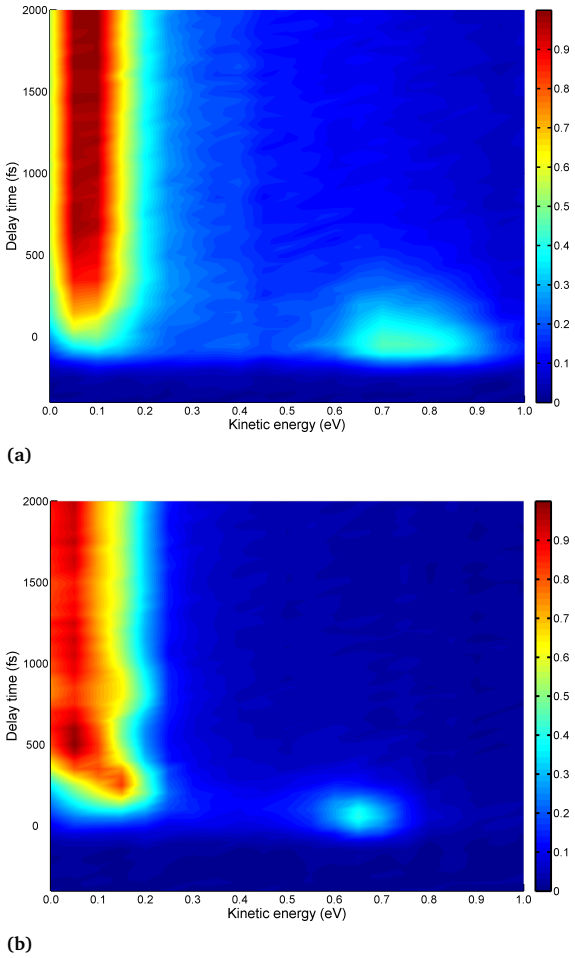

Fig. 3 TRPEI spectrum of (a) NMI and (b) NMM, measured with a pump wavelength of 200 nm and a probe wavelength of 400 nm. The small peak at early times corresponds to an excitation to the n→3p manifold. After internal conversion, the 3s state is populated (the peak at a lower kinetic energy that extends beyond 2 ps.

is less efficient in NMI than in NMM. The lifetime for the NMM 3p state is 135 fs which agrees well with the reported lifetime of 106 fs [11], when one takes into account the longer instrument response time of c.a. 160 fs in the current experiment.

The observed oscillations can be seen in figure 5, and an oscillation period of 600 fs has been determined. This is in good agreement with Zhang et al. [11] who reported an oscillation period of 630 fs.

The most striking observation is that there are no oscillations in the NMI spectrum. Following Zhang et al. [11] this suggests that the difference in topology between the 3s and D_0 surfaces is small.

As one can see in the difference plots in figure 6, the Rydberg state PES is not identical to that of the ground state ion in NMI or NMM. The figure shows a plot of the difference in energy between 3s and D_0, following the amine wagging mode; neither of these plots results in a flat line (or something close to that), suggesting that the surfaces are not parallel. If the coherences were preserved along the amine wagging mode in NMI, just as it is in NMM, it should be possible to see oscillations in the signal, especially as the energy difference falls comfortably within

Molecule	Conformer	Structure	Relative Energy (eV)	Electronic State	$3p_x$ excitation energy (eV)	Point group
NMM	Equatorial chair	(a) 1.	0	$1^1A'$	6.23	C_s
	Axial chair	(a) 2.	0.31	$1^1A'$	5.51	C_s
	Equatorial boat	(a) 3.	0.35	1^1A	6.07	C_1
	Axial boat	(a) 4.	0.42	1^1A	5.70	C_1
NMI	Equatorial chair	(b) 5.	0.01	1^1A	6.30	C_1
	Axial chair	(b) 6.	0	1^1A	6.12	C_1
	Equatorial boat	(b) 7.	0.27	1^1A	5.56	C_1
	Axial boat	(b) 8.	0.28	1^1A	6.03	C_1

Table 1 Relative energies of ground state minima in NMM and NMI. The energies for each regioisomer are reported respectively as relative to their most stable conformer. The value in the "structure" column gives the reference for the corresponding representation in figure 1.

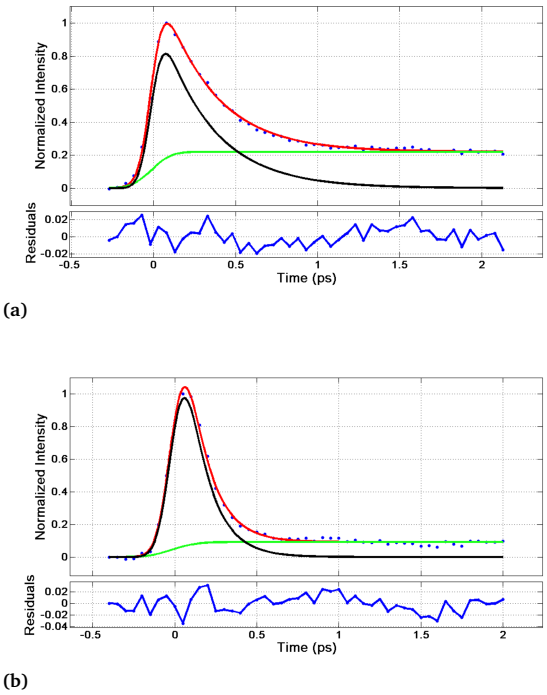

Fig. 4 Fits of the 3p to 3s decay in each system, where (a) shows NMI and is a fit of the decay between 0.5 eV and 1 eV, and (b) shows NMM where the decay has been fitted between 0.5 eV and 0.9 eV. Each graph shows that as time progresses, the population of the 3p state (red) exponentially decays into the 3s state (green). The black curve shows the fitted instrument response function.

Molecule	τ_{IC} (fs)	Oscillation period (fs)
NMM	135	600
NMI	312	-

Table 2 Fitted time constants

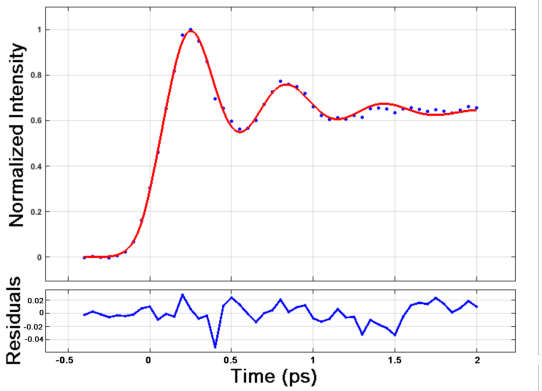

Fig. 5 Observed oscillations in NMM, where the blue points represent measured data, and the red line is the fit (fit between 0.15 eV and 0.3 eV).

the limits of the energy resolution of the detector. The fact that no oscillatory motion is observed in the measured spectrum of NMI indicates that the energy from the pump pulse likely spreads through many modes, rather than being confined.

The diffuse nature of the initially prepared wavepacket that is observed in the 3p peak for NMI, when compared to NMM, in figure 3 shows that the molecule can be excited to a greater number of vibronic states in NMI. The longer lifetime is an indication that the difference between the molecules is twofold - there are fewer accessible vibronic states in NMM, and there is also a lesser degree of coupling between the accessible states. This allows us to see that the excited state dynamics in NMM are more ballistic and directed as it moves towards the 3s state.

These experimental observations can be rationalised by using theoretical data and group theory. NMI has C_1 symmetry, and there are no possible conformers where it would have any other higher-order symmetry. Therefore, there are no symmetry restrictions on which vibronic transitions are allowed. This explains why a much more diffuse spectrum for NMI is observed, compared to NMM, as the only limiting factor here is which states are energetically available. This can be seen by expressing the transition dipole moment $\boldsymbol{d}_{n\to n'}$ as

$$\boldsymbol{d}_{n\to n'} = \langle \Psi_n | \boldsymbol{\mu} | \Psi_{n'} \rangle \langle \Theta_v | \Theta_{v'} \rangle \quad (4)$$

where Ψ_n is the wavefunction of the initial electronic state, n, $\boldsymbol{\mu}$ is the dipole operator, $\Psi_{n'}$ is the wavefunction of final electronic state, n'. Θ_v is the wavefunction of the initial vibrational state on the electronic ground state, v, and $\Theta_{v'}$ is the wavefunction of the final vibrational state on the electronically excited state, v'. As can be seen from this equation, in a C_1 molecule, none of the vibronic transitions can be necessarily excluded using symmetry, as the only irreducible representation is A. However, the symmetry of NMM causes it to differ quite significantly from NMI, in terms of symmetry allowed transitions. The ground state minimum of NMM is C_s, as are the global minima on the 3s and 3p Rydberg states. The molecule has a mirror plane and therefore values for the overlap integrals that are necessarily zero, so no transition to

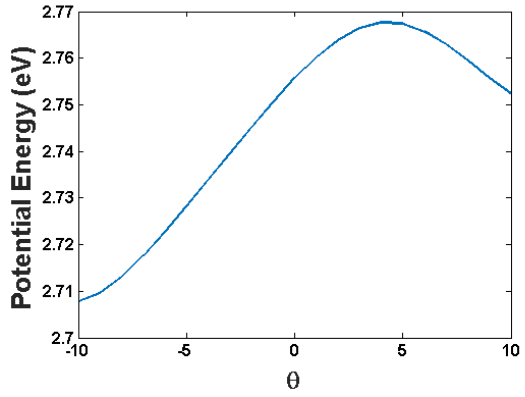

(a)

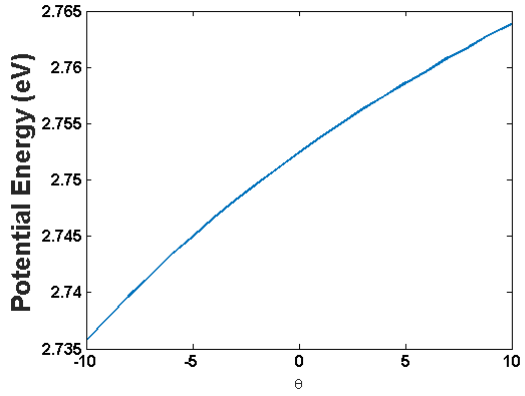

(b)

Fig. 6 Rydberg binding energy of the 3s Rydberg state of (a) NMM and (b) NMI, following the amine wag. Calculated at the CAM-B3LYP/6-311++G(d,p) level of theory.

between the corresponding states can occur.

3.2 Characterisation of the CI

Based on Fermi's Golden Rule, equation 1, it would be expected that a molecule with a greater density of vibronic states in the receiving electronic state would undergo internal conversion faster than one with a lesser vibronic state density[41]. As there are no symmetry restrictions for transitions between electronic states in NMI, one could reasonably expect that this would naturally lead to a faster rate of internal conversion, whilst there are symmetry restrictions to which transitions between electronic states can occur in NMM because only a' vibrational modes can couple two electronic states of $^1A'$ symmetry. However, it is clear that this is not the case in NMI and NMM by the lifetimes in table 2. Additionally, it is important to consider the energy gap between the two electronic states between which internal conversion is occurring - as this also has an impact on the lifetime of the higher lying state. At the Franck-Condon region, the energy gaps between the 3s and 3p states are 0.53 eV and 0.55 eV in NMM and NMI, respectively. Whilst NMI does have a larger energy gap, the difference is very small. It is not likely that an energy gap difference of 0.02 eV would be responsible for an internal conversion process that is three times slower.

Instead, the reason for the faster internal conversion in NMM than in NMI is that there is a CI that is formed along the methyl wagging and C-N stretching modes, connecting the 3p $^1A'$ to the 3s $^1A'$ states. The C-N stretch causes a significant Rydberg-valence mixing, which allows the 3p states to cross the 3s state. This Rydberg-valence mixing is demonstrated by an analysis of the CASSCF orbitals at the intersection geometry. From figure 7 it can be seen that the 3s Rydberg orbital becomes more localised over the methyl group, from the more uniform dispersion it has in the Franck-Condon region. It also acquires significant σ^* character, demonstrating the mixing. From a natural orbital analysis of the CI geometry, the occupation of the 3s orbital shown in 7(b) is 0.20, and the occupation of the σ^* state 7(c) is 0.28.

Figure 8 shows the characterisation of the CI for the $3p_x \rightarrow 3s$ transition. Both figure 8(a) and (b) were plotted using the following equation:

$$E^A(r,\theta), E^B(r,\theta) = E^X + \delta_{gh} r[\sigma cos(\theta - \theta_s) \pm \sqrt{1 + \Delta_{gh} cos(2\theta)}] \quad (5)$$

Where δ_{gh} describes the pitch of the intersection, Δ_{gh} gives the asymmetry, θ_s is defined as the direction in which the CI is tilted, and σ is the relative tilt of the intersection with regards to the branching plane. The energy E^X is the energy of the intersection geometry, and the energies E^A and E^B are the energies of the upper and lower surfaces, respectively. The distance r and angle θ are standard polar coordinates in the branching plane, where the optimised geometry of the intersection point is the origin[40].

Molecule	Excited State	State	$f_{f \leftarrow i}$
NMM	3s	$^1A'$	0.0120
	$3p_x$	$^1A''$	0.0041
	$3p_y$	$^1A'$	0.1159
	$3p_z$	$^1A'$	0.0318
NMI	3s	^1A	0.0242
	$3p_x$	^1A	0.0329
	$3p_y$	^1A	0.0778
	$3p_z$	^1A	0.0172

Table 3 Oscillator Strengths from the ground state to each of the four lowest lying Rydberg states in both NMM and NMI.

We can see from figure 8 that the CI is characterised as sloped bifurcating because the energy of the upper surface dips below the intersection energy, and there are two directions by which there is a negative gradient. In the 2D plot, figure 8(a), the branching space is defined in terms of $\hat{\mathbf{x}}$ and $\hat{\mathbf{y}}$. These are obtained by normalising the usual branching space that a CI is described in, by the following equations:

$$\hat{\mathbf{x}} = \frac{\tilde{\mathbf{g}}}{\sqrt{\tilde{\mathbf{g}} \cdot \tilde{\mathbf{g}}}} \; ; \quad \hat{\mathbf{y}} = \frac{\tilde{\mathbf{h}}}{\sqrt{\tilde{\mathbf{h}} \cdot \tilde{\mathbf{h}}}} \quad (6)$$

Where $\tilde{\mathbf{g}}$ and $\tilde{\mathbf{h}}$ are the vectors that usually form the branching space around a CI, as is outlined by Galván et al.[40].

The displacement vectors in figure 8(a) demonstrate that the branching vector $\hat{\mathbf{y}}$ follows the amine wagging motion, whilst following $\hat{\mathbf{x}}$ shows the C-N bond extension. It is evident that the

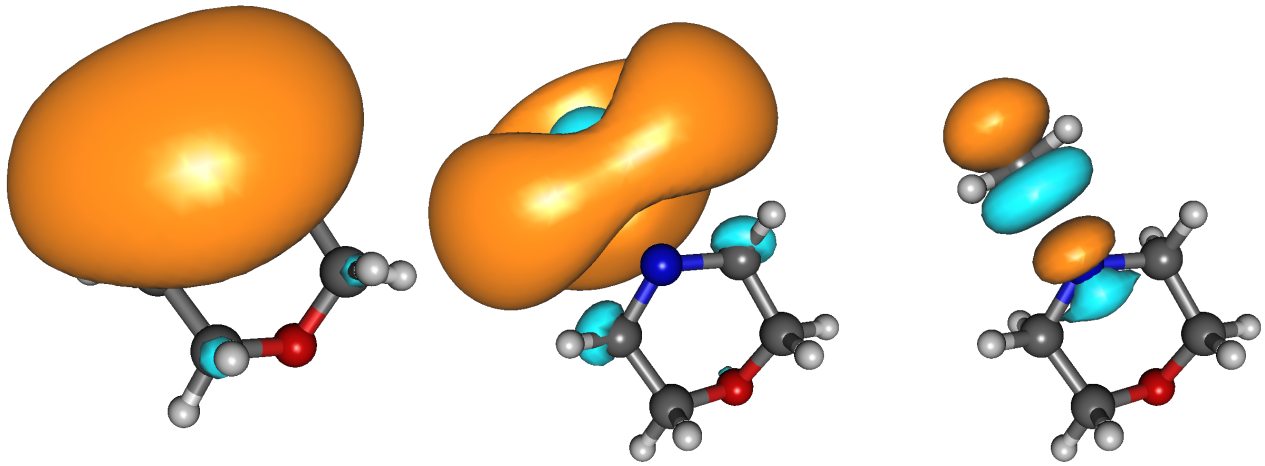

(a) (b) (c)

Fig. 7 NMM orbitals calculated at the CASSCF(12,12)/aug-cc-pVTZ level of theory, shown here are (a) the 3s orbital as it appears at the Franck-Condon region, (b) Rydberg-valence mixing of 3s and σ^*, shown by the significant distortion of the Rydberg orbital surrounding the methyl group, caused by electron density with σ^* character. (c) Shows the σ^* orbital of the N$-$CH$_3$ bond.

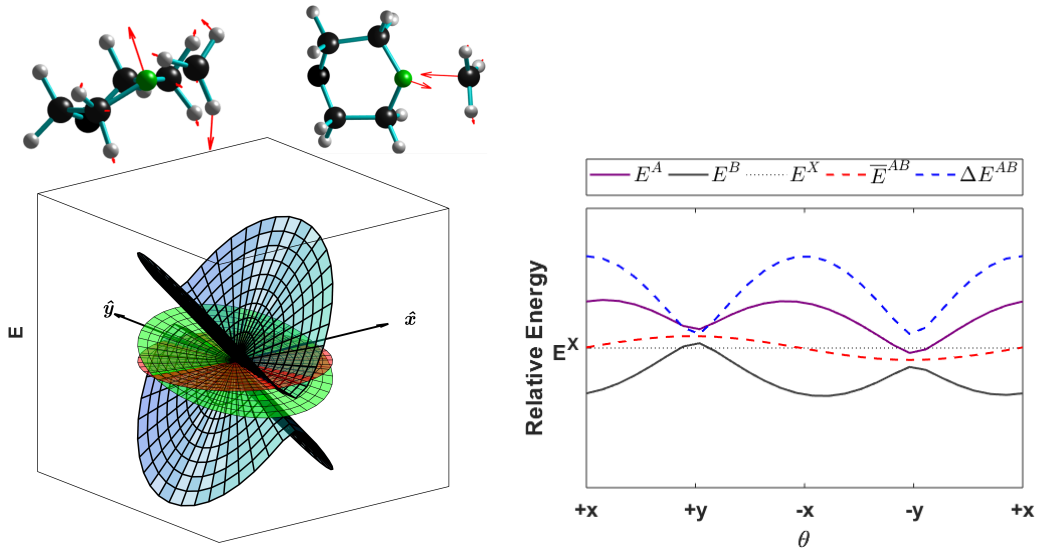

(a) (b)

Fig. 8 Characterisation of the conical intersection between the 3p and 3s states in NMM, calculated at the CASSCF(12,12)/aug-cc-pVTZ level. (a) shows the local representation of the intersection in terms of the polar coordinates r and θ. The red circle shows the energy of the optimised intersection geometry (E^X), the green circle shows how the average energy ($\overline{E}^{AB}$) of the upper and lower surfaces changes as a function of the vectors $\hat{\mathbf{x}}$ and $\hat{\mathbf{y}}$, which are themselves normalised vectors of the branching space vectors, $\tilde{\mathbf{g}}$ and $\tilde{\mathbf{h}}$, respectively. The inset chemical structures represent show porcupine plots of the $\hat{\mathbf{x}}$ vector (right) and of the $\hat{\mathbf{y}}$ vector (left), (b) shows how the energy of the intersection changes depending on θ for a fixed value of r, $\overline{E}^{AB}$ shows the average energy of the upper and lower surfaces, whilst ΔE^{AB} gives the difference in energy between the two.

system reaches the CI through a combination of the amine wagging and methyl stretching modes. This supports the notion that a CI is responsible for the 3p→3s ultrafast internal conversion in NMM, and confirms the validity of the results of the TD-DFT calculations.

3.3 Symmetry Analysis

Table 3 shows the oscillator strengths between the ground state and Rydberg states for NMM and NMI, which are proportional to the strength of the transition dipole moments. As discussed previously, the ground state symmetry of NMM is C$_s$ with a molecular electronic state symmetry of $^1A'$. The excited states of interest are the 3s, 3p$_x$, 3p$_y$, and 3p$_z$ states where the coordinates are defined as shown in figure 1. 3p$_x$ has a molecular electronic state symmetry of $^1A''$, whilst the other three excited states of interest

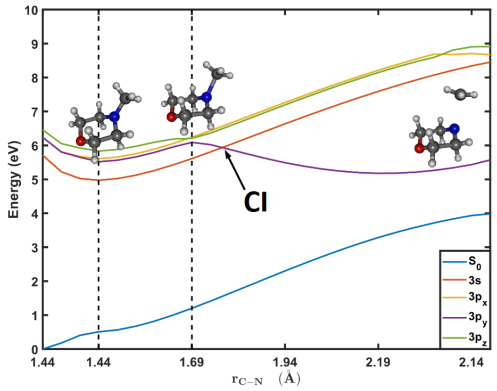

(a)

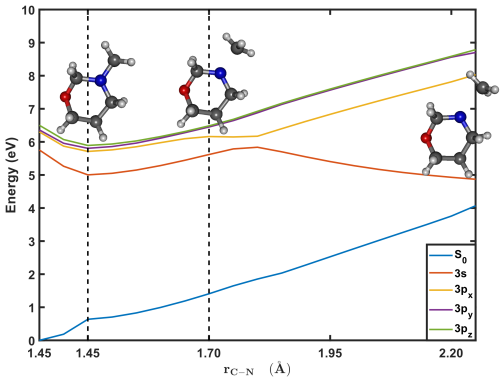

(b)

Fig. 9 Relaxed scan on the 3s surface of a CN stretching coordinate for a) the methyl group in NMM, and b) the NC-4 stretch in NMI calculated at the CAM-B3LYP/6-311++G(d,p) level of theory. The left black dotted line on both graphics shows the Franck-Condon region and is coinciding with the 3s minimum. Once the 3s minimum is reached, the linear axis then scales linearly. The right black dotted line demonstrates the length at which the CN bond has been distorted to the point where Rydberg-valence interactions become significant. The electronic states in NMM were assigned by examining the electronic state symmetry of each point for each excited state.

are $^1A'$. This means that $3p_x$ will be significantly less populated than $3p_y$ and $3pz$, as the transition dipole moment for $3p_x \leftarrow S_0$ has only one non-zero component, μ_x, whilst the transition dipole moment from a $^1A'$ state to another $^1A'$ state will have non-zero components of both μ_y and μ_z. As is shown by the surfaces in figure 9(a), the $3p_x$ and $3p_y$ states are very close in energy (with a difference in excitation energy of 0.004 eV), and the fact that there is no residual population observed in the TRPEI spectrum in figure 3(b) indicates that any population in an electronic state of $^1A''$ likely collapses to $^1A'$. This is also indicated by a geometry optimisation on each of the four Rydberg states, which results in one geometry with C_s symmetry, and a molecular electronic state symmetry of $^1A'$ on each of the four Rydberg states. There seems to be a barrier on 3p states prior to entering the CI region of the potential energy surface. This barrier is most likely a result of the relaxation being on the 3s state which on the other hand means that the 3p states are not showing the lowest energy paths.

Figure 10 shows the PES following a planarisation normal mode in (a) NMM and (b) NMI. As one can see, the planarisation in each molecule takes the excited state away from the Franck-Condon region at 0° because the gradient leading to a more planar structure is negative. Despite this, it is also evident that there are no conical intersections or avoided crossings found following the potential energy surface along this vibrational mode, so it cannot account for the ultrafast internal conversion alone even though it is the path of steepest descent towards the excited state minima.

The minimum energy structures in the 3s Rydberg states of NMM and NMI are shown in figure 11. As the Rydberg states are near parallel to each other in the absence of valence mixing, the minima are very similar in the 3s state and each of the 3p states. Figure 11, structure 10. shows the global minimum on the 3s Rydberg state in NMM, which has C_s symmetry. Structure 9. relates to another minimum with C_1 symmetry, the relation is very similar to that on the ground state where boat-like structures are connected as well. On the 3s surface, the energy gap between these two minima is 0.1 eV, as the ground state symmetry is C_s, and the 3s global minimum is also C_s, it is implied that NMM never breaks symmetry throughout its dynamics. In the two NMI structures, 11. and 12., the only minimum that is accessible under normal conditions is structure 12. which is lower in energy and is the excited state minimum that is located when starting from one of the two chair conformers on the ground state, whereas structure 11. is reached when starting from a boat geometry. Both 11. and 12. are very similar in energy, with 12. being slightly more stable by 0.02 eV in the 3s state.

Because the initial 3p population rapidly becomes entirely $^1A'$, and the symmetry of the 3s state whilst the molecule is in C_s symmetry is also $^1A'$, only a' normal modes can facilitate internal conversion. As there is a minimum of C_1 symmetry on each 3p surface, as well as the 3s surface, it has to be considered whether the system passes through this minimum; when the PES for each Rydberg state is examined at the Franck-Condon region, and following each of the 3N-6 normal modes, it is seen that the modes along which there is a steep descent leading away from the Franck-Condon region for each of the three 3p states are modes pertaining to the planarisation of the nitrogen - mainly the wagging motion of the methyl group, and the planarisation mode. These have a' symmetry and therefore cannot lead to the C_1 minimum, suggesting that this minimum is not relevant to the internal conversion.

When investigating the N-Me bond stretch on the 3s surface, a crossing was discovered between the $3p_y$ and 3s states in NMM and an avoided crossing in NMI. The C-N stretching introduces significant valence character that results in a CI with coupling to the amine wagging motion and the N-Me stretching coordinate. The progression that takes NMM through the CI is a non-ergodic process, due to the symmetry restrictions upon both the optical transitions and any subsequent transitions between electronic states. The path of steepest descent out of the Franck-Condon region follows the planarisation of the nitrogen atom along a 3p $^1A'$ surface, which then forms an accidental same-symmetry CI with the 3s $^1A'$ surface. These modes pass through the C_s minimum,

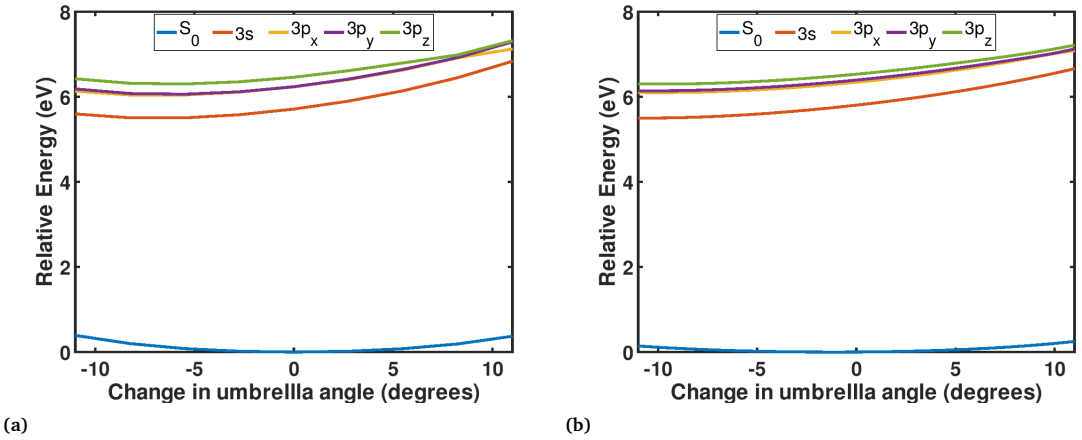

Fig. 10 PES following a planarisation vibrational mode in (a) NMM and (b) NMI where 0° in both figures is the Franck-Condon region and a negative change in the umbrella angle is moving towards a more planar amino group. Calculated at the CAM-B3LYP/6-311++G(d,p) level of theory.

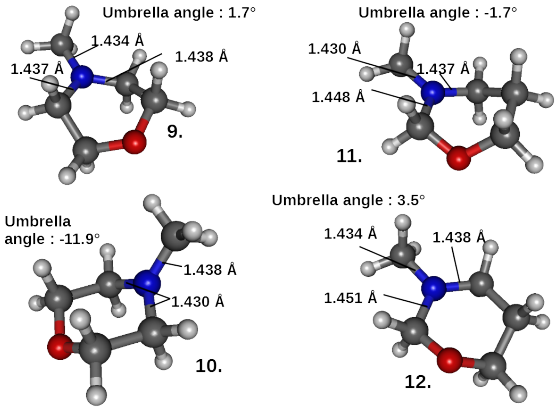

Fig. 11 Structures and geometric data for the 3s Rydberg state for NMM and NMI. As in figure 1, the umbrella angle gives the planarisation of the nitrogen atom, where a value of 0° implies that the nitrogen centre is completely planar.

though they are not able to take the system to the C_1 minimum. In NMI, however, this is not the case as there are no symmetry restrictions on the system. This means that the system will move around the PES ergodically, but still according to the path of steepest descent, because there are no vibronic modes that are necessarily excluded in the optical transition. In this way, there is a clear rationalisation for the somewhat surprising behaviour of a symmetric system decaying significantly faster than a system of lower order symmetry.

The relaxed CN bond scans shown in figure 9 used TD-DFT (CAM-B3LYP/6-311++G(d,p)). The structures were optimised for the 3s Rydberg state, since its population is of interest here. In NMM, Rydberg-valence mixing becomes important at 1.69 Å. C_s symmetry is preserved throughout the entire scan, and the wagging motion is shown to happen alongside the stretching motion, as demonstrated by the inset structures in figure 9(a). The transformation of these structures show how the molecule transforms in the local representation of $\hat{\mathbf{x}}$ and $\hat{\mathbf{y}}$ in figure 8(a). The change in the ONC(H_3) angle from the 3s minimum to the point where the Rydberg-valence interaction becomes noticeable is 10.2°, after which point the lowest lying 3p surface becomes a repulsive σ^* surface. The energy of this point is 6.09 eV, which is accessible when the system is excited with a 200 nm pulse. The other CN stretches in NMM do not need to be considered, as these are a'', and therefore would not be able to couple the 3p and 3s surfaces.

For NMI, there are no symmetry restrictions on how the energy can disperse into the modes that would be available to couple the 3p manifold and the 3s Rydberg state alongside the CN stretch, as the point group of NMI is always C_s so there is only ever the single irreducible representation A. Accordingly, similar behaviour is observed for each of the three possible CN stretches, with the only differences being the barrier heights where the surfaces change from attractive to repulsive. It is also the case that the N−CH_3 stretch in NMI appears to form an avoided crossing, rather than a CI - therefore differing from both NMM and the other two CN stretches in NMI that do form CIs. For each of the three stretches the distance where the Rydberg-valence mixing becomes most important is always around 1.70 Å, although the most energectically favourable stretch is the N−CH_3 stretch, for which the peak is 6.16 eV. Given that a 200 nm pulse corresponds to c.a. 6.20 eV, the system is excited with enough energy to reach this point. Interestingly, the scan of the N−CH_3 bond in NMI shows no dependence on the wagging motion corresponding to the planarisation of the nitrogen centre, it only shows that the methyl twisting motion, and a wagging motion in the plane of the molecule, occur in concert with the stretching motion. This gives us an indication as to why the internal conversion in NMI follows a more statistical regime: the system explores the surface statistically according to a path of steepest descent, as there are no symmetry restrictions involved regarding the initial population of the vibronic states. The most favourable motion that the system initially follows is the planarisation because the minima on both the 3s and 3p states have a planarised nitrogen. The planarisation of the nitrogen centre is the path of steepest descent out of the Franck-Condon region, but for internal conversion to occur,

more degrees of freedom have to be involved because the 3p and 3s surfaces do not couple when only following the planarisation of either molecule. As there are symmetry restrictions to the initial excitation in NMM, the system is confined within certain degrees of freedom. The symmetry of NMM also means that only normal modes of a certain symmetry can couple the 3p and 3s states. In NMI, there are no such symmetry restrictions, therefore the system is not confined to how it explores the 3p PES meaning that it explores it statistically, which rationalises the Fermi behaviour of NMI compared to the non Fermi behaviour of NMM because Fermi's Golden Rule only applies when the excited state dynamics of a system are statistical. We cannot completely rule out that part of reason for the slower dynamics in NMI is due to the fact that symmetry does not allow for the formation of a CI but rather an avoided crossing.

The difference in ergodicity between the NMM and NMI systems is further backed up by theoretical calculations of the Rydberg binding energy as a function of the amine wagging motion in both NMM and NMI they depend on the umbrella angle, indicating that one should be able to see oscillations in the time-resolved spectra of both molecules. In fact, when following the Rydberg binding energy as a function of any of the normal modes in either system, it is seen that no motion has a zero gradient, indicating that the Rydberg states are not identical to D_0. The fact that this is the case makes the absence of oscillations in the NMI spectrum surprising.

In summary, the excited state dynamics in NMM result from these symmetry effects because the transition from the 3p to the 3s state involves only a' vibronic modes, mainly the amine wagging motion, so the molecular motion is preserved in these oscillations. In addition to this, the oscillations are preserved because the global minimum on the 3s state - much like the 3p states - has C_s symmetry, the electronic state of which is $^1A'$. Indeed, the C_1 minimum is close in energy to the global minimum, however, the system reaches the 3s state following a $^1A'$ electronic surface and the C_1 minimum has an electronic state of ^1A. The only modes that are able to couple these two surfaces are necessarily a'' vibrational modes, as these motions break the symmetry. But there can be no crossing from 3p to 3s following a'' normal modes as that would result in an overlap integral between the 3p and 3s that would be necessarily zero because both states that are coupling are $^1A'$. While the $3p_x$ state is the lowest lying 3p Rydberg state in the Franck-Condon region according to the TD-DFT calculations, the stationary point located on the lowest-lying 3p Rydberg surface retains the C_s point group and has an electronic state symmetry of $^1A'$. Upon reflection on these inconsistencies, it appears as though either this level of theory gets the state ordering of the 3p Rydberg states qualitatively wrong at the Franck-Condon region (regardless of the very good agreement with CASPT2 calculations and experimental results), or that the initial population is predominately prepared in the $3p_{y,z}$ states and the 3p state ordering changes at the slightest deformation, resulting in $3p_y$ being the lowest-lying 3p Rydberg state. As $3p_y$ has an electronic state symmetry of $^1A'$, the 3s and 3p manifold are therefore allowed to couple following symmetric a' vibrational modes. One indicator that the state ordering is incorrect is the fact that $3p_x$ is the lowest-lying 3p Rydberg state only at initial excitation, after this single point $3p_y$ becomes the lowest-lying Rydberg state. As of this moment, the early time dynamics in the 3p manifold are still unclear, though the fact remains that the initial preparation of the excited state population is far more favourable in electronic states with a symmetry of $^1A'$, and only symmetric vibrational modes are able to couple two electronic states of the same symmetry, meaning that only a' modes can take the NMI $3p_{y,z}$ population to the 3s state. The system therefore continues to transform by the a' normal modes after internal conversion, as these are the only modes that are able to couple the two states. The oscillations are preserved on 3s because these are the only modes that are populated after internal conversion, meaning that there is no population transfer into the a'' modes. Given that the a'' modes would result in the NMM being taken to a minimum that is higher-lying in energy than the C_s minimum, these oscillations are observed in the NMM TRPEI spectrum in figure 3(b), and disappear over time as the energy disperses throughout the degrees of freedom in the molecule as it relaxes into the 3s C_s global minimum.

4 Conclusions

Through combined experimental and computational results it is demonstrated that there is a regioisomeric dependence on the observation of preserved vibrational coherences. By changing the ring position of the oxygen atom, symmetry is lost, which destroys the vibrational coherence. Stationary points have been identified and characterised, giving greater insight into what is driving ultrafast internal conversion. We have shed light on this striking phenomenon and an understanding of two isomeric systems (NMM and NMI) has been built up to the point where it is shown that, fundamentally, symmetry is a controlling factor. With consideration of previous literature, it is not possible at this stage to put forward an argument claiming that this is a general rule applicable to the excited state dynamics of the Rydberg states of all tertiary aliphatic amines. However, the observations made and subsequent analysis demonstrate that symmetry effects in large systems can drastically affect the excited state dynamics.

The work presented here gives insight into designing molecules to direct their excited state dynamics along certain degrees of freedom. It is demonstrated that, by changing the symmetry of these two systems, the excited state dynamics can be radically altered. In NMM the entire excited state population is funnelled from one state to another through very few degrees of freedom, giving rise to coherent oscillations, whilst in NMI this behaviour is completely nullified. Therefore, by paying attention to the symmetry of a system it might be possible to tune the excited state dynamics of a molecule. This subtle control could be utilised in the design of solar cells, for example, by designing a molecule in such a way as to limit motions in normal modes that are able to couple surfaces - increasing the lifetime of the excited state, and therefore having the potential to increase the efficiency of energy transfer.

Conflicts of interest

There are no conflicts to declare.

Acknowledgements

We are grateful to Martina Cacciarini for help with optimizing the synthetic workup of NMI. We also extend many thanks to Hannes Jónsson, Mátyás Pápai, and Klaus B. Møller for stimulating discussions concerning the theory. PMW acknowledges support from the Army Research Office (Grant No. W911NF-17-1-0256).

Notes and references

1 S. Iuchi and N. Koga, *Physical Chemistry and Chemical Physics*, 2016, **18**, 4789–4799.

2 T. I. Sølling, T. S. Kuhlman, A. B. Stephansen, L. B. Klein and K. B. Møller, *ChemPhysChem*, 2014, **15**, 249–259.

3 D. R. Yarkony, *Reviews of Modern Physics*, 1996, **68**, 985–1013.

4 H.-G. Duan and M. Thorwart, *The Journal of Physical Chemistry Letters*, 2016, **7**, 382–386.

5 A. D. Hammerich, U. Manthe and R. Kosloff, *The Journal of Chemical Physics*, 1994, **101**, 5623–5646.

6 D. Keefer, S. Thallmair, S. Matsika and R. de Vivie-Riedle, *Journal of the American Chemical Society*, 2017, **139**, 5061–5066.

7 T. S. Rose, M. J. Rosker and A. H. Zewail, *J. Chem. Phys.*, 1989, **91(12)**, 7415–7436.

8 K. Munkerup, D. Romanov, T. Bohinski, A. B. Stephansen, R. J. Levis and T. I. Sølling, *J. Phys. Chem. A*, 2017, **121**, 8642–8651.

9 F. Ling, S. Li, X. Song, Y. Wang, J. Long and B. Zhang, *Scientific Reports*, 2017, **7**, 15362.

10 R. Monni, G. Auböck, D. Kinschel, K. M. Aziz-Lange, H. B. Gray, A. Vlček and M. Chergui, *Chemical Physics Letters*, 2017, **683**, 112–120.

11 Y. Zhang, H. Jónnson and P. Weber, *Phys. Chem. Chem. Phys.*, 2017, **19**, 26403–26411.

12 B. J. Whitaker, *Science*, 2011, **334**, 187–188.

13 K. Jorner, A. Dreos, R. Emanuelsson, O. E. Bakouri, I. F. Galván, K. Börjesson, F. Feixas, R. Lindh, B. Zietz, K. Moth-Poulsen and H. Ottosson, *Journal of Materials Chemistry A*, 2017, **5**, 12369–12378.

14 M. Ndong, L. Bomble, D. Sugny, Y. Justum and M. Desouter-Lecomte, *Physical Review A*, 2007, **76**, 043424.

15 X. Yang, T. Keane, M. Delor, A. J. Meijer, J. Weinstein and E. R. Bittner, *Nature Communications*, 2017, **8**, 14554–1–14554–8.

16 F. Sterpone, R. Martinazzo, A. N. Panda and I. Burghardt, *Zeitschrift für Physikalische Chemie*, 2011, **225**, 541–551.

17 I. Hwang and G. D. Scholes, *Chemistry of Materials*, 2011, **23**, 610–620.

18 T. Nelson, A. Naumov, S. Fernandez-Alberti and S. Tretiak, *Chemical Physics*, 2016, **481**, 84–90.

19 T. R. Nelson, D. Ondarse-Alvarez, N. Oldani, B. Rodriguez-Hernandez, L. Alfonso-Hernandez, J. F. Galindo, V. D. Kleiman, S. Fernandez-Alberti, A. E. Roitberg and S. Tretiak, *Nature Communications*, 2018, **9**, 2316–1–2316–8.

20 P. M. Shenai, S. Fernandez-Alberti, W. P. Bricker, S. Tratiak and Y. Zhao, *Journal of Physical Chemistry B*, 2016, **2016**, 49–58.

21 D. R. Yarkony, *J. Chem. Phys.*, 1990, **92**, 2457–2463.

22 F. Bernardi, M. Olivucci, J. Michl and M. A. Robb, *The Spectrum*, 1996, **9**, 1–6.

23 F. Bernardi, M. Olivucci and M. A. Robb, *Acc. Chem. Res.*, 1990, **23**, 405–412.

24 F. Bernardi, S. De, M. Olivucci and M. A. Robb, *J. Am. Chem. Soc.*, 1990, **112**, 1737–1744.

25 M. Koch, B. Thaler, P. Heim and W. E. Ernst, *The Journal of Physical Chemistry A*, 2017, **121**, 6398–6404.

26 W. K. Peters, D. E. Couch, B. Mignolet, X. Shi, Q. L. Nguyen, R. C. Fortenberry, H. B. Schlegel, F. Remacle, H. C. Kapteyn, M. M. Murnane and W. Li, *PNAS*, 2017, **114**, E11072–E11081.

27 J. L. Gosselin, M. P. Minitti, F. M. Rudakov, T. I. Sølling and P. M. Weber, *J. Phys. Chem. A*, 2006, **110**, 4251–4255.

28 W. A. Chupka, *The Journal of Chemical Physics*, 1987, **87**, 1488–1498.

29 L. B. Klein, T. J. Morsing, R. A. Livingstone, D. Townsend and T. I. Sølling, *Phys. Chem. Chem. Phys.*, 2016, **18**, 9715–9723.

30 L. B. Klein, J. O. F. Thompson, S. W. Crane, L. Saalbach, T. I. Sølling, M. J. Paterson and D. Townsend, *Phys. Chem. Chem. Phys.*, 2016, **18**, 25070–25079.

31 L. B. Klein and T. I. Sølling, *Chemical Physics*, 2014, **442**, 62–67.

32 A. R. Allouche, *Journal of Computational Chemistry*, 2011, **32**, 174–182.

33 A. R. Katritzky, V. J. Baker and F. M. S. Brito-Palma, *J. Chem. Soc., Perkin Trans. 2*, 1980, **0**, 1739–1745.

34 S. Lias, J. Bartmess, J. Liebmann, J. Holmes, R. Levin and W. Mallard, *NIST Chemistry WebBook, NIST Standard Reference Database number 69*.

35 S. Lias, *NIST Chemistry WebBook, NIST Standard Reference Database number 69*.

36 M. J. Frisch, G. W. Trucks, H. B. Schlegel, G. E. Scuseria, M. A. Robb, J. R. Cheeseman, G. Scalmani, V. Barone, G. A. Petersson, H. Nakatsuji, X. Li, M. Caricato, A. V. Marenich, J. Bloino, B. G. Janesko, R. Gomperts, B. Mennucci, H. P. Hratchian, J. V. Ortiz, A. F. Izmaylov, J. L. Sonnenberg, D. Williams-Young, F. Ding, F. Lipparini, F. Egidi, J. Goings, B. Peng, A. Petrone, T. Henderson, D. Ranasinghe, V. G. Zakrzewski, J. Gao, N. Rega, G. Zheng, W. Liang, M. Hada, M. Ehara, K. Toyota, R. Fukuda, J. Hasegawa, M. Ishida, T. Nakajima, Y. Honda, O. Kitao, H. Nakai, T. Vreven, K. Throssell, J. A. Montgomery, Jr., J. E. Peralta, F. Ogliaro, M. J. Bearpark, J. J. Heyd, E. N. Brothers, K. N. Kudin, V. N. Staroverov, T. A. Keith, R. Kobayashi, J. Normand, K. Raghavachari, A. P. Rendell, J. C. Burant, S. S. Iyengar, J. Tomasi, M. Cossi, J. M. Millam, M. Klene, C. Adamo, R. Cammi, J. W. Ochterski, R. L. Martin, K. Morokuma, O. Farkas, J. B. Foresman and D. J. Fox, *Gaussian 16 Revision A.03*, 2016, Gaussian Inc. Wallingford CT.

37 T. Yanai, D. P. Tew and N. C. Handy, *Chemical Physics Letters*, 2004, **393**, 51–57.

38 B. G. Levine, C. Ko, J. Quenneville and T. J. Martínez, *Molec-*

ular Physics, 2006, **104**, 1039–1051.

39 F. Aquilante, J. Autschbach, R. K. Carlson, L. F. Chibotaru, M. G. Delcey, L. D. Vico, I. F. Galván, N. Ferré, L. M. Frutos, L. Gagliardi, M. Garavelli, A. Giussani, C. E. Hoyer, G. L. Manni, H. Lischka, D. Ma, P. Å. Malmqvist, T. Müller, A. Nenov, M. Olivucci, T. B. Pedersen, D. Peng, F. Plasser, B. Pritchard, M. Reiher, I. Rivalta, I. Schapiro, J. Segarra-Martí, M. Stenrup, D. G. Truhlar, L. Ungur, A. Valentini, S. Vancoillie, V. Veryazov, V. P. Vysotskiy, O. Weingart, F. Zapata and R. Lindh, *Journal of Computational Chemistry*, 2016, **37**, 506–541.

40 I. F. Galván, M. G. Delcey, T. B. Pedersen, F. Aquilante and R. Lindh, *Journal of Chemical Theory and Computation*, 2016, **12**, 3636–3653.

41 T. S. Kuhlman, M. Pittelkow, T. I. Sølling and K. B. Møller, *Angewandte Chemie International Edition*, 2013, **52**, 2247–2250.